Mongolian Geoscientist

Original paper

Geochemistry of mafic extrusive lavas in the Bayankhongor Ophiolite, Mongolia

Bayarmaa Batsukh[1,3], Turbold Sukhbaatar[1,2*], Gerel Ochir[2], Oyunbold Sukhbaatar[1], Odgerel Dashdorjgochoo[1]

[1]Institute of Geology, Mongolian Academy of Sciences, Ulaanbaatar 18080, Mongolia
[2]Geoscience Center, Mongolian University of Science and Technology, Ulaanbaatar 14191, Mongolia
[3]Department of Geology and Geophysics, School of Arts and Sciences, National University of Mongolia, Ulaanbaatar 14191, Mongolia

*Corresponding author: turbold_s@mas.ac.mn, ORCID: 0000-0002-4788-2923

ARTICLE INFO

Article history:

Received: 23 April, 2025
Revised: 11 September, 2025
Accepted: 14 September, 2025

ABSTRACT

This study presents new geochemical data on pillow lavas from the Bayankhongor Ophiolite in western Mongolia, revealing compositions that range from sub-alkaline to alkaline basalts. While most of these basalts are tholeiitic, some show transitional geochemical variations. Except for one sample resembling normal mid-ocean ridge basalt, all others are enriched in light rare earth elements and closely resemble enriched mid-ocean ridge basalt and ocean island basalt. The presence of high-field strength elements such as Th, Ta, Nb, Zr, Hf, and Ti indicates a mantle-derived origin. Tectonic discrimination diagrams demonstrate a transition between enriched mid-ocean ridge basalt and within-plate basalt, characteristic of mid-ocean ridges. The samples are categorized into three groups based on the LREE variation: low- normal mid-ocean ridge basalt, high-enriched mid-ocean ridge basalt, and ocean island basalt, suggesting advanced partial melting of the mantle and a mixing of mid-ocean ridge basalt with ocean island basalt. The Bayankhongor Ophiolite is widely recognized as a subduction-unrelated ophiolite and represents one of the largest Neoproterozoic oceanic rift basins in the Central Asian Orogenic Belt. Consequently, subduction-unrelated tectonic models are often favored for the Bayankhongor Ophiolite, which somewhat aligns with our findings. However, recent studies highlight the importance of subduction-related models and timing. Our model aims to integrate both aspects.

Keywords: Pillow lava, EMORB, OIB

INTRODUCTION

The Central Asian Orogenic Belt (CAOB), also called the Altaids (Şengör et al., 1993, 2022), formed over a long time range, starting at the beginning of the Tonian and continuing until the upper Triassic (Şengör et al., 2022; Windley et al., 2007; Zonenshain, 1973), and includes a variety of lithologically distinct rock complexes that naturally occur in nearly all geotectonic settings described in geology, such as ophiolites, arcs, accretionary wedges, and microcontinents (Windley et al., 2007). This complex geological structure which developed over a long period spans the entire CAOB (Windley et al., 2007), also called Altaids (Şengör et al., 1993, 2022). The CAOB is a large subduction-accretion complex sandwiched between the Siberian craton in the north and the Tarim and North Chinese cratons in the south (Şengör et al., 1993, 2022; Windley et al., 2007). It has recently been referred to as a "Supercollage" which includes the Mongolian Collage to the east, the Kazakhstan Collage to

the west, and the Tarim-North China Collage to the south (Xiao et al., 2018 and references therein). The Mongolian Collage, for instance, is primarly composed of Paleozoic arc-related rock and accretionary complexes that exhibit oroclinal bending structure on a crustal scale (Parfenov et al., 2003; Xiao et al., 2015). In addition, the Central Mongolian Massive (CMM) within the Mongolian Collage contains fragments of the Precambrian microcontinent including the Baidrag, Zavkhan, Tuva-Mongol, and Tarvagatai Blocks (Tomurtogoo, 2014). The southern part of the CMM is represented by the Baidrag Block and is connected to the enormous oceanic basin in the north, known as the Bayankhongor Ophiolite (BRO) in the Bayankhongor Zone (BZ). This oceanic lithosphere has been distinctly named either the Paleo-Asian Ocean (Terent'eva et al., 2008, 2010) or the Palaeo-Pacific Ocean (Sukhbaatar et al., 2024 and references therein) and is composed of rocks with mid ocean ridge (MOR)-like Nd-Sr isotopic compositions (epsilon $Nd_{(t)}$ = +7.6 to +4.7; Jian et al., 2010). Jian et al. (2010) interpreted that this oceanic crust formed overnearly 100 Ma, and has geological characteristics similar to subduction-related, Cordilleran-type ophiolite (Wakabayashi and Dilek, 2003). In contrast, recent studies suggest that the BRO corresponds to an ophiolite that is subduction-unrelated (Furnes and Safonova, 2019; Jian et al., 2010), contrasting with earlier works suggesting a subduction influence (Buchan et al., 2002). However, the lavas present in the BZ may have formed in both tectonic settings, just at different times. For instance, Sukhbaatar et al. (2024) presented a revised interpretation of the Ediacaran (ca. 564-598 Ma) active margin in the northeastern part of the Baidrag Block.

In this work, we aim to contribute to the geochemistry of the mafic extrusive rocks from the BRO, which is crucial to understanding the geotectonic evolution of the BZ within the CAOB.

GEOLOGICAL SETTING

The BZ is often regarded as an oceanic basin, dominated by fragments of late Neoproterozoic (zircon U-Pb data of ca. 636-665 Ma; Jian et al., 2010; Kovach et al., 2005) remnants of ophiolite (Badarch et al., 2002; Buchan et al., 2002; Jian et al., 2010; Tomurtogoo, 1989, 2014). The mafic to ultramafic rocks within the BZ are called the BRO, which is one of the largest dismembered ophiolite mélanges in the CAOB (Jian et al., 2014; Windley et al., 2007). The ophiolite mélange consists of serpentinites, cumulate rocks, gabbros, pillow lavas, sheeted dykes, and deep marine sediments, including cherts (Badarch et al., 2002; Jian et al., 2010; Tomurtogoo, 1989, 2014). In present day coordinates, the BZ exhibits a narrow structure (~ 80 km wide) between the Tarvagatai Block in the north and the BB in the south, extending approximately 300 km from northwest to southeast (Buchan et al., 2002; Demoux et al., 2009 and references therein). However, the northern margin is unclear and is mostly covered by Devonian-Carboniferous turbidites known as the Khangai Basin (Zorin, 1999), which was later emplaced by Permian-Triassic felsic intrusions (Jahn et al., 2004; Yarmolyuk et al., 2019). Notably, Buchan et al. (2001) interpreted the northern part of the BZ attached to the passive margin that is represented by the NW-SE extending narrow zone belt called the Zag Zone. Prior to the Paleozoic geological events, the Bayankhongor oceanic crust was subducted beneath the Baidrag Block by its southward subduction (~ 564-598 Ma; Sukhbaatar et al., 2024). Sukhbaatar et al. (2024) interpreted that the volcanic rocks from the Ulziit Gol Unit (UGU) in the BZ compositionally range from basaltic to felsic and exhibit both MORB-like and subduction-influenced geochemical characteristics, similar to volcanic rocks found in a back-arc basin (Pearce and Stern, 2006). Those subduction-related volcanic rocks of the UGU display distinct structural, lithological, and geochemical characteristics compared to the basaltic rocks (mostly pillow lavas) of the BRO (Sukhbaatar et al., 2024; Terent'eva et al., 2008, 2010). For instance, the UGU mainly consists of a volcanic-sedimentary sequence sourced from both the Ediacaran juvenile arc in the BZ and Precambrian Baidrag Block in the south (Sukhbaatar et al., 2024), while the basaltic lavas from the BRO are primarily part of the ophiolite section, such as the serpentinite

mélange (Terent'eva et al., 2008; Jian et al., 2014). Due to a later tectonic event, the oceanic fragments of the BRO were thrust over the northeastern margin of the BB, forming its current structure (Buchan et al., 2001, 2002).

METHODS

In total, we analyzed 14 basaltic rock samples (pillow-like lavas) collected along the Bayankhongor ophiolite zone, from southeast to northwest. The locations and modal compositions of the studied samples are reported in Table 1. In the field, we collected about 2-3 kg of rocks for each sample. The samples were crushed and homogenized at the Institute of Geology, Mongolian Academy of Sciences in Ulaanbaatar and analysed at the SGS IMME Mongolia LLC laboratory (https://www.sgs.com/en) using procedures of GE-ICP40Q1 package (ICP-OES method) and GE-ICP40Q package (ICP-MS method) for trace elements (for 40 and 20 elements, respectively using the four-acid digestion). The geochemical data are plotted using the GCDkit 6.2 package (Janoušek et al., 2006, updated in 2022; see the following link: www.gcdkit.org)

PETROGRAPHY

We sampled mafic extrusive rocks from the BRO, as shown in Fig. 1. The mineral assemblages and coordinates of analysed samples are provided in Table. 1.

The basaltic lavas display various forms (Fig. 2), and are commonly associated with ultramafic-mafic rocks and parallel dyke complexes (Figs. 2A-C). They exhibit pillow-like structures in the field (Figs. 2D, E); however, in some cases, the basaltic lavas are brecciated (Fig. 2F). The lavas consist of primary amphibole and plagioclase, as well as, secondary minerals such as actinolite, magnetite, epidote, and serpentine (Figs. 3C, D). Two samples are not lavas. Sample BHR2417C is serpentinite predominatly composed of serpentine,

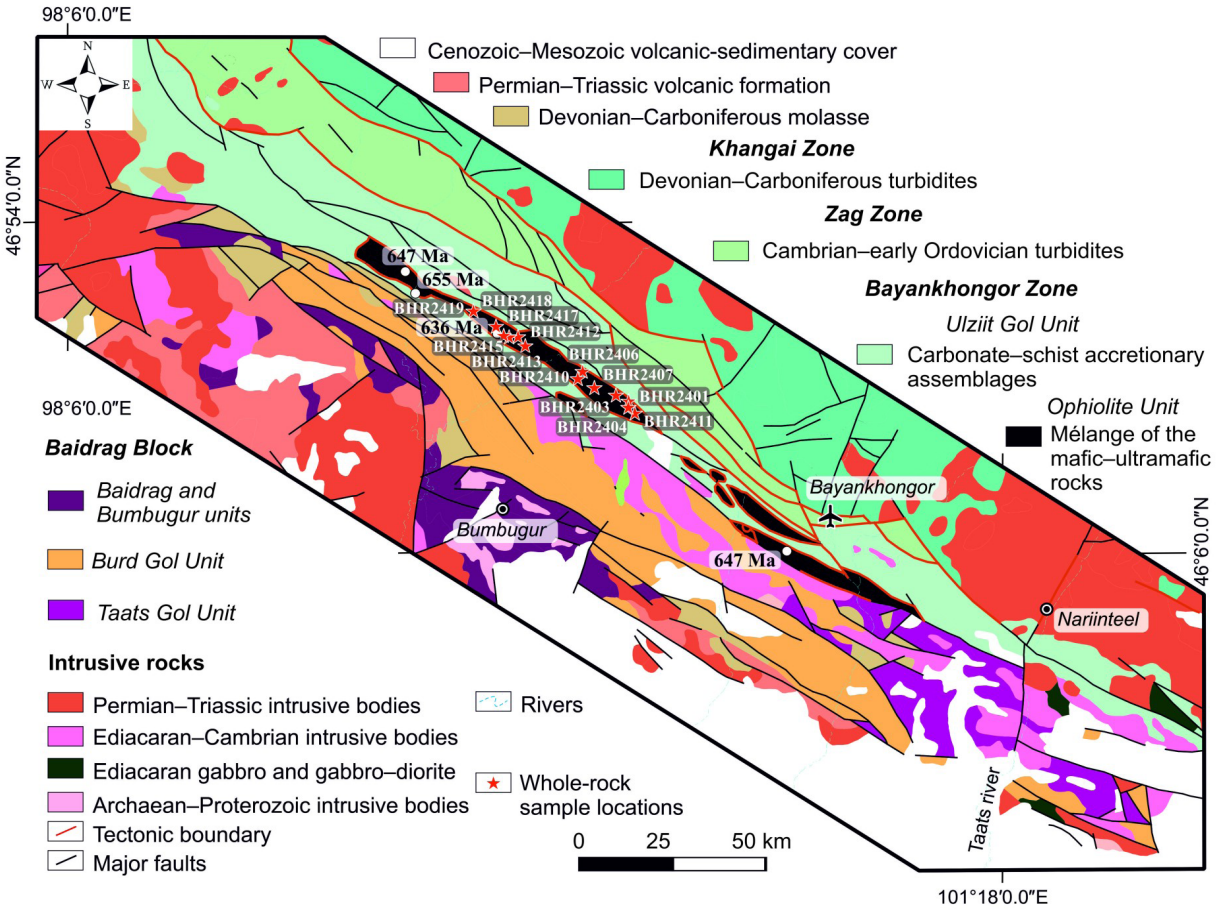

Fig. 1. Simplified tectonic map of the Bayankhongor area in western Mongolia (Sukhbaatar et al., 2024). Locations of previous geochronological studies are indicated by white circles (Jian et al., 2010), while samples from this work are represented by red stars with sample numbers.

Table 1. General description of the mineral assemblage and location of the analyzed sample from the BRO.

Sample	Rock name	Mineral assemblage	Latitude	Longitude
BHR2401	Tuff lava	Pl, tuffitic matrix	46.5010	99.9690
BHR2403	Porphyritic basalt	Pl, secondary Cal, Chl, vein of Ms	46.5105	99.9366
BHR2404	Basalt	Pl, Amp, Chl, Vein of Ms	46.5054	99.9444
BHR2404B	Basalt	Pl, Amp	46.5054	99.9444
BHR2406	Basalt	Pl, Ep	46.5488	99.8631
BHR2407	Basalt	Pl, Amp	46.5258	99.8565
BHR2410	Basalt	Pl, Ep	46.5282	99.8400
BHR2412	Porphyritic basalt	Pl, Amp	46.6257	99.6434
BHR2413	Amphibole bearing basalt	Pl, Amp, Chr, Ep, Mag	46.6244	99.6400
BHR2415	Porphyritic basalt	Pl, Cpx, Amp, secondary Mag, Chl, Mus	46.6078	99.6357
BHR2417A	Amphibole bearing basalt	Hbl, Pl	46.6114	99.6258
BHR2418	Metabasalt	Amp, Pl, secondary Ep, Chl	46.6240	99.6037
BHR2419	Fine-grained basalt	Pl, Amp	46.6623	99.5133
BHR2422	Basalt	Pl, Amp, secondary Chl		

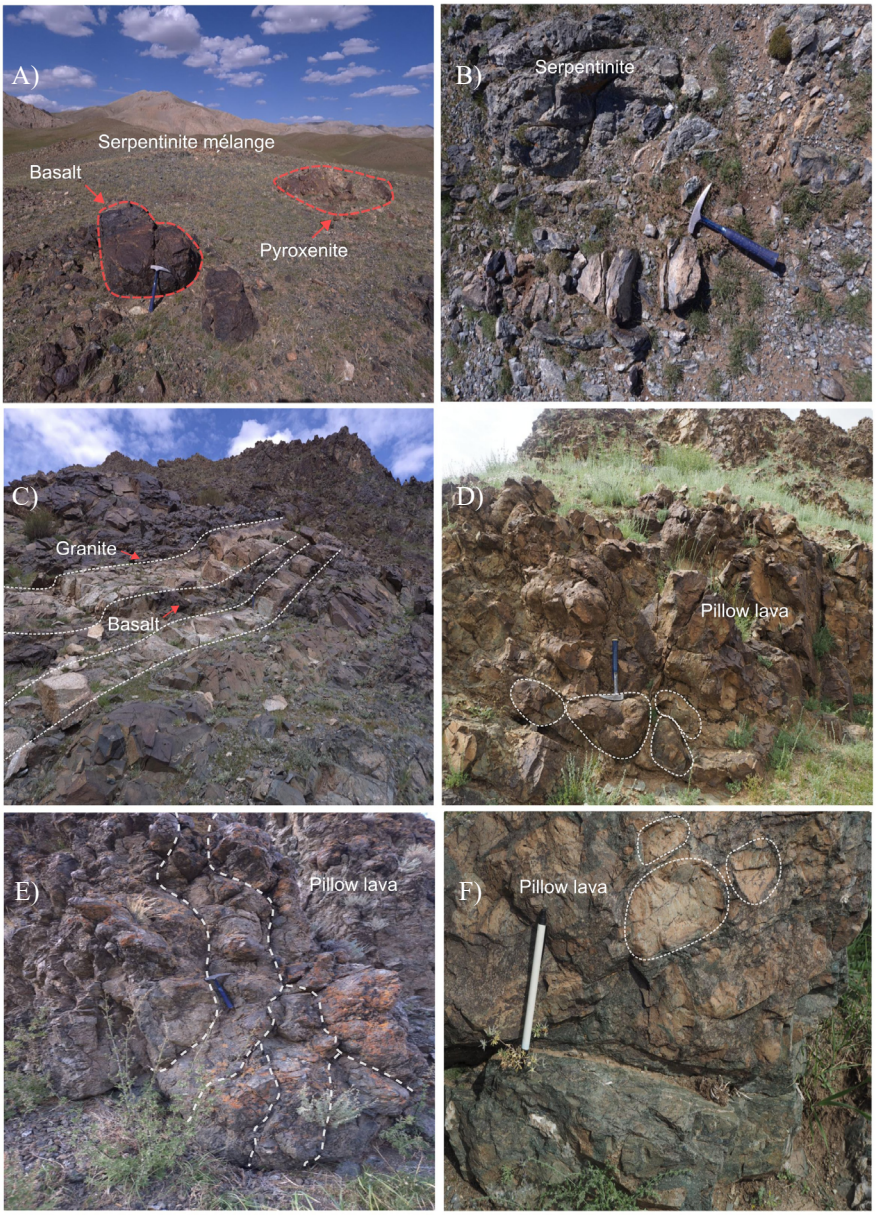

Fig. 2. Field photographs of extrusive volcanic rocks from the Bayankhongor area. A) A boudin of intrusive ultramafic and mafic extrusive rocks enclosed within a serpentine mélange. B) Serpentinite that constitutes the ophiolite mélange. C) Felsic parallel dykes crosscut the basaltic lava. D-E) Lavas with pillow-like structures. F) Volcanic breccia featuring a hyaloclastic matrix.

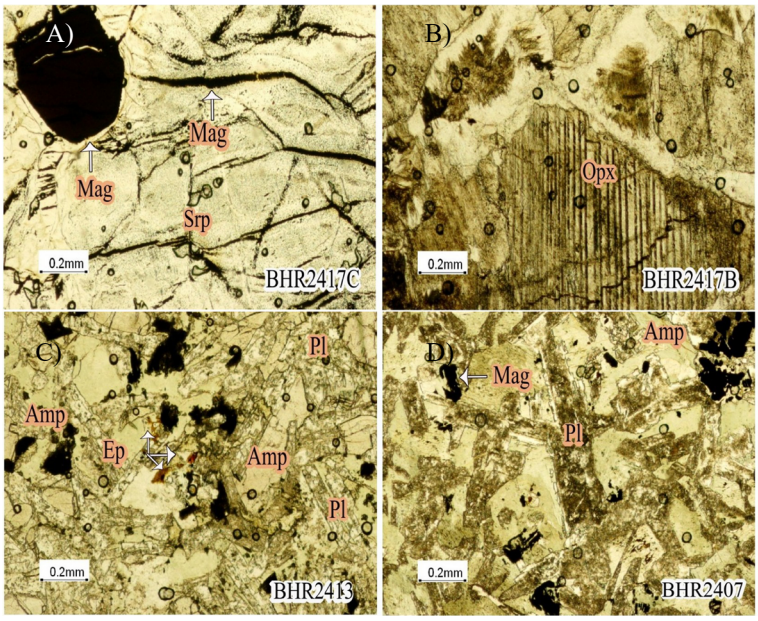

Fig. 3. Microphotomicrographs of rocks collected from the BRO: A) Serpentinite; B) Pyroxenite; C) Amphibole-bearing basalt; D) Basalt. The abbreviation is based on the work of Whitney and Evans (2010).

chromite, and magnetite (Fig. 3A), while the pyroxenite sample BHR2417B consists of both ortho- and clinopyroxenes, partially overprinted by serpentine (Fig. 3B). The rock formations in the BZ, including the studied basaltic lavas, were affected by regional metamorphism at greenschist to lower amphibolite facies. For instance, ultramafic rocks are commonly altered to serpentinite, which is a major rock type representing ultramafic rocks, and forms the ophiolite mélange (Figs. 2A, B, and 3A, B).

GEOCHEMISTRY

For whole-rock geochemistry, we analysed 14 basaltic rock samples from the BRO. The modal compositions are reported in Table 1, and geochemical data are provided in Table. 2.

Rock Classification

Based on some high field strength element (HFSE) that are used as indicator elements (Zr and Nb) to identify the alkalinity of rocks, we split our samples into three groups: Group 1 has a low concentration of Zr and Nb (Zr=16.7 ppm, Nb=0.8 ppm), while Group 2 contains moderate levels of Zr and Nb (Zr=43.5-131.0 ppm, Nb=3.7-13.8 ppm). In contrast, Group 3 is characterized by high levels of Zr and Nb, with concentrations ranging from 126.0 to 183.0 ppm for Zr and 22.3 to 60.6 ppm for Nb. Group 1 includes a single sample BHR2417A, which is amphibole-rich, fine-grained basalt, while Group 2 represents ten basaltic samples. Unlike the others, Group 3 contains three samples that are alkali basalts (BHR2406, BHR2418, and BHR2419).

As the studied samples were affected by greenschist to lower amphibolite facies metamorphism after their formation, we focus primarily on the characteristics of immobile HFSE such as Zr, Nb, Y, and Ti to classify the rocks (Pearce, 1996). Overall, the samples exhibit a tholeiitic composition as indicated by the Zr/Y vs. Th/Yb diagram (Ross and Bédard, 2009), although some show a transitional composition towards a Zr-rich phase (Fig. 4B).

Characteristics of REE and Trace Elements

Fig. 5 displays the rare earth element (REE) and trace element concentrations of 14 basaltic samples normalized to chondritic meteorites (Boynton, 1984; Fig. 5A) and average composition of normal mid-ocean ridge basalt (NMORB) (Sun and McDonough,1989; Fig. 5B). In the following paragraph, the samples are categorized into three groups (see rock classification above), showing distinct patterns in their light rare earth element (LREE) (Fig. 5A). For all samples, the La_N/Sm_N ratios range from 0.63 to 4.28 and the Eu anomalies vary

Table 2. Chemical data for volcanic rocks from the BRO.

Sample name	BHR 2406	BHR 2418	BHR 2419	BHR 2401	BHR 2403	BHR 2404	BHR 2404B	BHR 2407	BHR 2410	BHR 2412	BHR 2413	BHR 2415	BHR 2417A	BHR 2422
Rock name	Basalt	Meta-basalt	Fine-grained basalt	Tuff lava	Porphyritic basalt	Basalt	Basalt	Basalt	Basalt	Porphyritic basalt	Basalt	Porphyritic basalt	Amphibole bearing basalt	Basalt
Geochemical classification	Alkaline			Subalkaline										
REE elements (ppm)														
La	14.2	25.9	45.6	13.3	4.2	11	10.9	9.9	10	7.4	7.8	4.6	1	14.8
Ce	32.6	54	85.4	26.4	8.51	25.2	24.4	22.4	21.5	16	17.4	10.3	2.41	29.7
Pr	4.36	7.3	10.1	3.68	1.31	3.73	3.56	3.13	3	2.3	2.54	1.52	0.43	3.75
Nd	21.2	33.2	41.5	17.4	6.5	18.6	18.2	15	14.5	11.4	12.5	7.7	2.5	17.1
Sm	4.8	6.6	6.7	4.1	1.9	4.8	4.6	3.5	3.5	3	3.5	2.1	1	3.7
Eu	1.56	2.14	2.1	1.48	0.76	1.58	1.5	1.21	1.27	1.16	1.21	0.78	0.38	1.57
Gd	5.4	7.3	5.8	5	2.5	6.2	6.1	4.4	4.7	3.9	4.5	2.8	1.6	4.2
Tb	0.95	1.22	0.97	0.93	0.52	1.16	1.1	0.84	0.82	0.73	0.87	0.52	0.34	0.7
Dy	5.46	7.12	5.63	5.45	3.28	7.59	7.01	5.08	5.33	4.79	5.43	3.51	2.53	4.32
Ho	1.19	1.4	1.11	1.21	0.72	1.66	1.54	1.16	1.2	1.03	1.2	0.7	0.56	0.89
Er	3.06	3.57	3.05	3.23	1.96	4.33	4.34	3.35	3.31	2.9	3.29	2.03	1.64	2.39
Tm	0.4	0.47	0.4	0.47	0.29	0.59	0.57	0.45	0.47	0.38	0.43	0.26	0.22	0.32
Yb	2.5	3.2	2.7	3	1.9	3.8	3.9	3.3	3.2	2.6	3.1	1.8	1.7	2.2
Lu	0.39	0.43	0.38	0.44	0.29	0.54	0.53	0.48	0.46	0.39	0.46	0.27	0.24	0.32
ΣREE	98.07	153.85	211.44	86.09	34.64	90.78	88.25	74.2	73.26	57.98	64.23	38.89	16.55	85.96
Eu/Eu*	0.94	0.94	1.03	1	1.07	0.89	0.87	0.94	0.96	1.03	0.93	0.98	0.92	1.22
LaN/YbN	3.83	5.46	11.39	2.99	1.49	1.95	1.88	2.02	2.11	1.92	1.7	1.72	0.4	4.54
LaN/SmN	1.86	2.47	4.28	2.04	1.39	1.44	1.49	1.78	1.8	1.56	1.4	1.38	0.63	2.52

Table 2. Chemical data for volcanic rocks from the BRO. continued

Sample name	BHR 2406	BHR 2418	BHR 2419	BHR 2401	BHR 2403	BHR 2404	BHR 2404B	BHR 2407	BHR 2410	BHR 2412	BHR 2413	BHR 2415	BHR 2417A	BHR 2422
Rock name	Basalt	Meta-basalt	Fine-grained basalt	Tuff lava	Porphyritic basalt	Basalt	Basalt	Basalt	Basalt	Porphyritic basalt	Basalt	Porphyritic basalt	Amphibole bearing basalt	Basalt
Geochemical classification	Alkaline			Subalkaline										
Other element (ppm)														
Ag	<2	<2	3	<2	<2	<2	<2	<2	<2	<2	<2	<2	<2	<2
Al (%)	8.59	8.71	9.09	8.72	11.48	8.93	8.89	8.82	8.55	11.12	9.31	10.98	8.11	9.08
Ba	259	7	3	117	240	23	52	172	113	285	43	120	37	2635
Ca (%)	8.36	13.86	>15	3.34	8.59	6.8	7.36	6.73	8.19	7.45	8.01	10.06	9.77	9.05
Cr	93	60	145	289	236	85	60	45	46	111	91	227	1072	94
Cu	83.4	53.9	<0.5	47.9	55.3	<0.5	<0.5	45.1	64.4	44	63.5	44.2	71.8	54.3
Fe (%)	9.7	10.78	8.92	9.84	5.8	9.61	9.17	9.54	8.97	6.95	9.56	5.98	6.58	7.89
K (%)	1.1	0.01	0.01	0.37	0.77	0.05	0.21	0.63	0.3	1	0.09	0.48	0.06	0.05
K	11000	100	100	3700	7700	500	2100	6300	3000	10000	900	4800	600	500
Li	6	2	5	46	8	2	3	2	1	5	6	17	5	2
Mg (%)	3.22	3.94	4.42	5.8	3.47	3.68	3.73	3.73	4.03	3.24	4.14	3.09	8.79	4.63
Mn	1606	1859	1973	1684	1067	1324	964	1716	1706	1300	1721	1101	1229	1436
Na (%)	0.56	0.04	0.02	1.17	2.64	3.11	2.69	2.64	2.14	2.29	2.94	1.33	0.79	2.44
Ni	70	33	85	125	56	36	36	32	30	36	40	52	410	63
P (%)	0.13	0.21	0.21	0.11	0.04	0.15	0.12	0.1	0.09	0.07	0.09	0.05	0.01	0.08
S (%)	<0.01	<0.01	0.01	<0.01	<0.01	0.08	<0.01	0.04	0.02	0.09	0.16	<0.01	<0.01	<0.01
Sr	1770	212	19.6	62.6	265	171	144	186	199	186	111	224	56.8	1940
Ti (%)	1.33	2.07	1.61	1.24	0.56	1.36	1.32	1.04	0.93	0.78	1.1	0.62	0.34	1.04
Ti	13300	20700	16100	12400	5600	13600	13200	10400	9300	7800	11000	6200	3400	10400
V	311	436	253	282	177	277	319	340	310	240	334	194	176	278
Zn	94	117	47	102	53	34	20	84	87	75	99	55	51	73
Zr	126	183	169	125	43.5	131	82.8	96.2	58.8	65.8	93.9	48.8	16.7	85
Be	0.8	1.4	1.1	0.8	0.3	0.7	0.8	0.7	0.7	0.6	0.7	0.4	0.1	0.7
Sc	35.5	36.2	27.9	37.8	31.2	35.9	39.1	40.4	39.9	32.2	40.7	28.7	33.2	40.5

continued

Table 2. Chemical data for volcanic rocks from the BRO.

Sample name	BHR 2406	BHR 2418	BHR 2419	BHR 2401	BHR 2403	BHR 2404	BHR 2404B	BHR 2407	BHR 2410	BHR 2412	BHR 2413	BHR 2415	BHR 2417A	BHR 2422
Rock name	Basalt	Meta-basalt	Fine-grained basalt	Tuff lava	Porphyritic basalt	Basalt	Basalt	Basalt	Basalt	Porphyritic basalt	Basalt	Porphyritic basalt	Amphibole bearing basalt	Basalt
Geochemical classification	Alkaline			Subalkaline										
Co	45.3	42.4	42.1	51.5	30.7	40.9	38.6	43	42.1	32.1	41.1	25.6	55.9	46.2
Ga	18.4	19.2	12.4	19.3	15	20.9	21.1	18.1	17.9	18.1	17.6	16	11	18.7
Ge	0.3	0.1	0.2	0.5	0.4	0.4	0.3	0.4	0.4	0.3	0.3	0.2	0.6	0.3
As	<1	<1	<1	<1	<1	<1	<1	<1	<1	<1	<1	1	<1	<1
Se	<2	<2	<2	<2	<2	<2	<2	<2	<2	<2	<2	<2	<2	<2
Rb	27.1	0.2	0.3	12.2	14.1	1.2	4.3	14.4	6.6	20.1	1.8	10.8	1.3	1.7
Y	29.9	36.4	30.8	32	19.6	44.5	39.5	30.8	29.8	26.5	32	20.4	15.8	24.9
Nb	22.3	34.9	60.6	13.7	3.7	12.6	11.7	13.8	12.7	8.2	9.7	5.7	0.8	15
Mo	0.69	1.58	0.45	0.57	0.28	0.92	0.77	0.48	0.46	0.54	0.55	0.47	0.27	0.84
Cd	0.05	0.1	0.05	0.12	0.08	<0.02	<0.02	0.11	0.11	0.11	0.14	0.11	0.08	0.09
In	0.09	0.11	0.09	0.07	0.05	0.1	0.08	0.08	0.09	0.07	0.08	0.06	0.04	0.07
Sn	1.5	1.9	1.9	1.4	0.6	1.6	1.5	1.1	0.9	0.9	1	0.7	0.4	1.1
Sb	0.05	<0.05	<0.05	0.09	<0.05	<0.05	0.06	<0.05	<0.05	<0.05	<0.05	0.07	<0.05	<0.05
Te	<0.05	<0.05	<0.05	<0.05	0.06	<0.05	<0.05	<0.05	<0.05	<0.05	<0.05	<0.05	<0.05	<0.05
Cs	<1	<1	<1	<1	<1	<1	<1	<1	<1	1	<1	<1	<1	<1
Hf	3.33	5.05	4.8	3.16	1.37	3.71	2.89	2.73	1.94	2.02	2.55	1.37	0.66	2.6
Ta	1.63	2.44	4.17	0.97	0.39	0.87	0.83	1	0.94	0.68	0.7	0.45	0.16	1.08
W	0.3	0.4	0.5	0.9	0.1	0.4	0.4	0.2	0.4	0.2	0.2	0.4	<0.1	0.2
Re	<0.05	<0.05	<0.05	<0.05	<0.05	<0.05	<0.05	<0.05	<0.05	<0.05	<0.05	<0.05	<0.05	<0.05
Tl	0.05	<0.02	<0.02	0.08	0.04	<0.02	<0.02	<0.02	<0.02	0.05	<0.02	0.05	<0.02	<0.02
Pb	2.1	1.1	1	1.9	1	0.7	1.1	0.9	1.2	1.2	1.4	0.6	0.8	0.8
Bi	<0.04	<0.04	<0.04	<0.04	<0.04	<0.04	<0.04	<0.04	<0.04	<0.04	<0.04	<0.04	<0.04	<0.04
Th	1.6	2.5	5.5	1.2	0.4	1	1.1	1.2	1.1	0.7	0.7	0.5	<0.2	1.3
U	0.32	0.72	1.45	0.37	0.12	0.31	0.29	0.3	0.27	0.18	0.24	0.1	<0.05	0.34

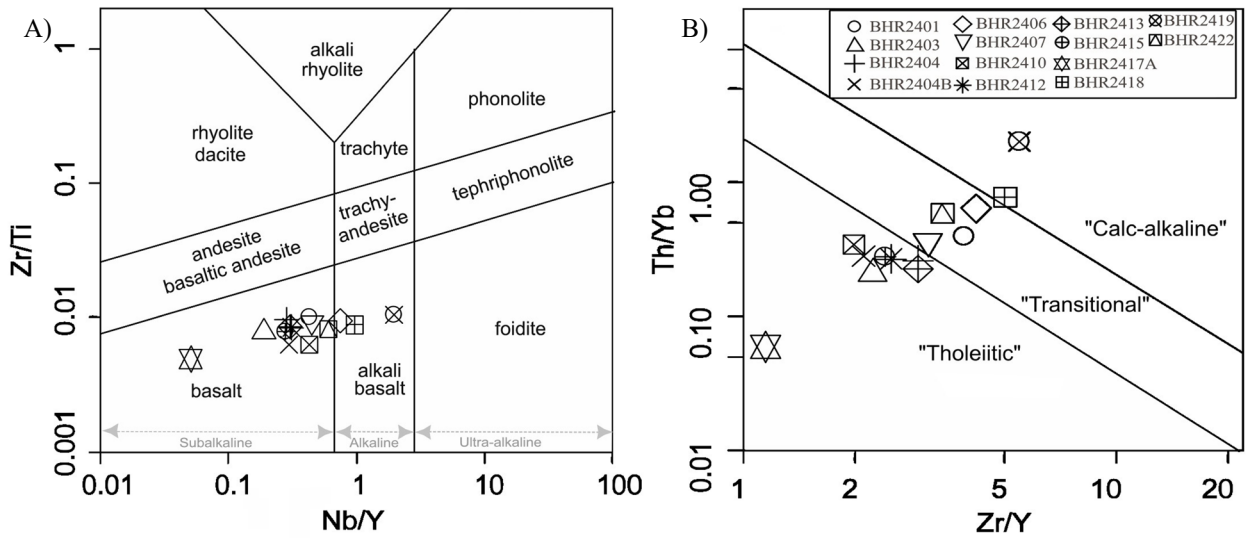

Fig. 4. Whole-rock geochemical classification diagrams for extrusive volcanic rocks of the BRO: A) Binary plot of Zr/Ti versus Nb/Y (Winchester and Floyd, 1977 - modified by Pearce, 1996). B) Zr/Y versus Th/Yb diagram modified by Ross and Bédard (2009).

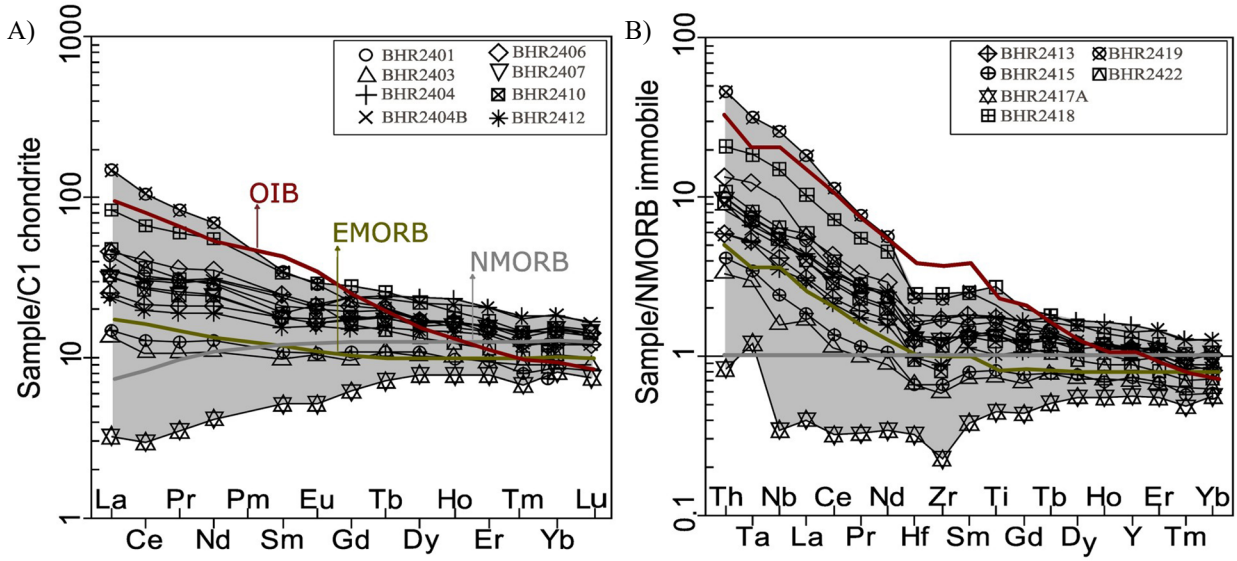

Fig. 5. A) Chondrite-normalized (Boynton, 1984) REE pattern, B) NMORB (Sun and McDonough, 1989, in Pearce, 2014) normalized spider plot.

from negative to positive (Eu/Eu*=0.86-1.21; see Table 2).

Amphibole-rich basaltic sample BHR2417A belongs to Group 1 and has the lowest content in its total REE (ΣREE=16.55). This sample also has a less La_N/Sm_N ratio (0.62), negative Eu anomaly (Eu/Eu*=0.92), and is depleted in LREE (La_N/Yb_N=0.40; see Table 2). Group 2 includes the 10 subalkalic basalts, which have higher total REE abundance (ΣREE =34.64-90.78) and La_N/Sm_N ratios (1.37-2.51) compared to Group 1. The Eu anomalies in these samples range from negative to positive (Eu/Eu*=0.86-1.21). In Fig. 5A, the samples exhibit varying levels of LREE (La_N/Yb_N=1.49-4.53; see Table 2). In contrast, three alkali basaltic samples (BHR2406, BHR2418, and BHR2419) exhibit the highest total REE concentrations (ΣREE =98.07-211.44), which influence the La_N/Sm_N ratios (1.86-4.28). Notably, these samples are significantly enriched in LREE (La_N/Yb_N=3.83-11.39) and their Eu anomalies are slight (Eu/Eu*=0.94-1.03; see Table 2). As a result, they display the highest levels of LREE, as illustrated in Fig. 5A. Nevertheless, the fluid-immobile elements Th and HFSE (Ta, Nb, Hf, Zr, and Ti) are present in higher concentrations in all samples (Fig. 5B).

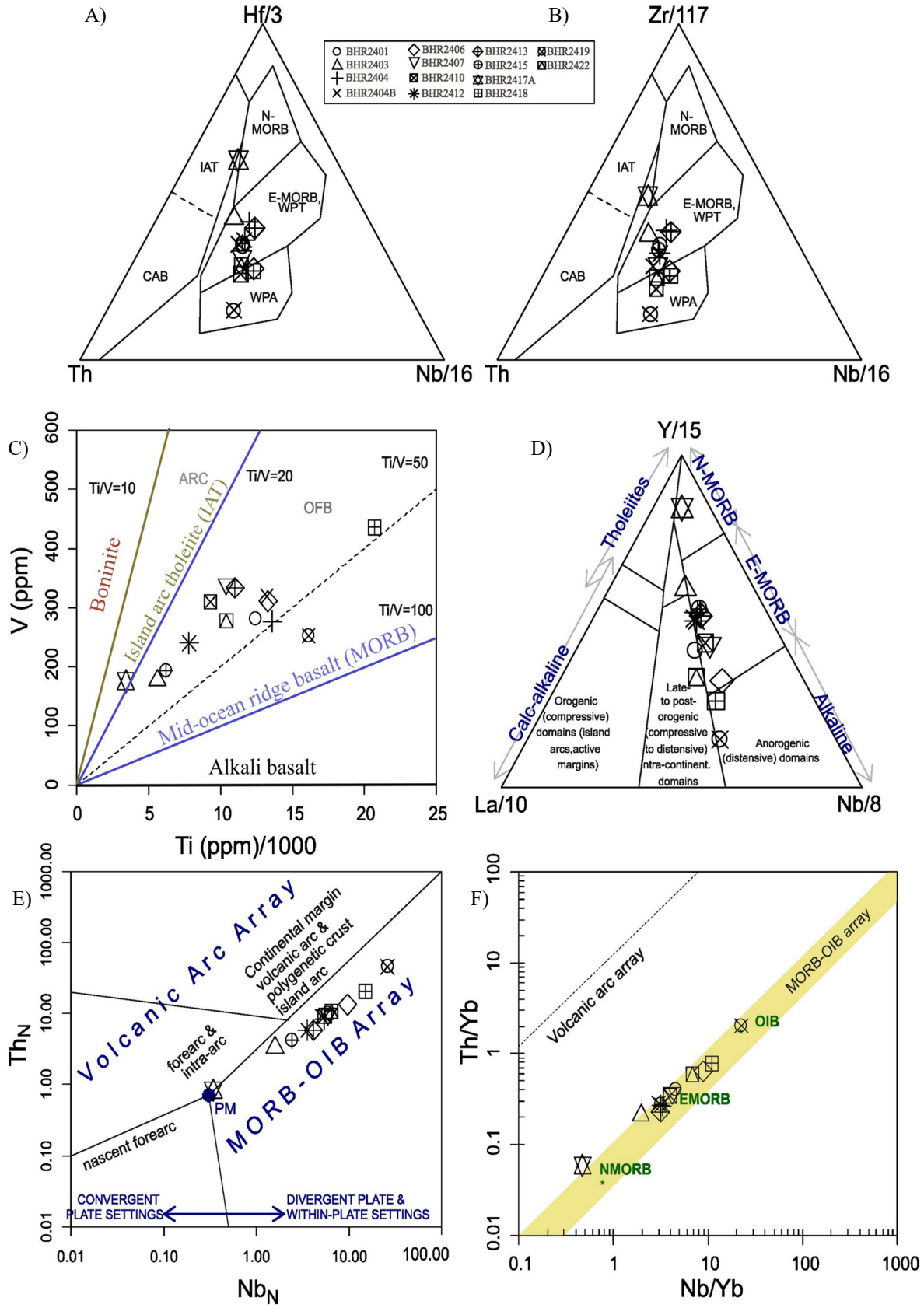

Fig. 6. Geotectonic discrimination diagrams for volcanic rocks from BRO include the following: A) Th-Hf/3-Nb/16 ternary plots (Wood, 1980). B) Th-Zr/117-Nb/16 triangular plot (Wood, 1980). C) Geochemical classification diagram of V vs. Ti (Shervais, 1982). D) Ternary diagram of La/10-Y/15-Nb/8 (Cabanis and Lecolle, 1989). E) Th_n vs. Nb_n diagram (Saccani et al., 2015). F) Nb/Yb vs. Th/Yb discrimination diagram (Pearce, 2008). Abbrevaition: CAB=Calc-Alkaline Basalts; IAT=Island-Arc Tholeiites; WPT=Within-Plate Tholeiites; WPA=Within-Plate Alkaline basalts.

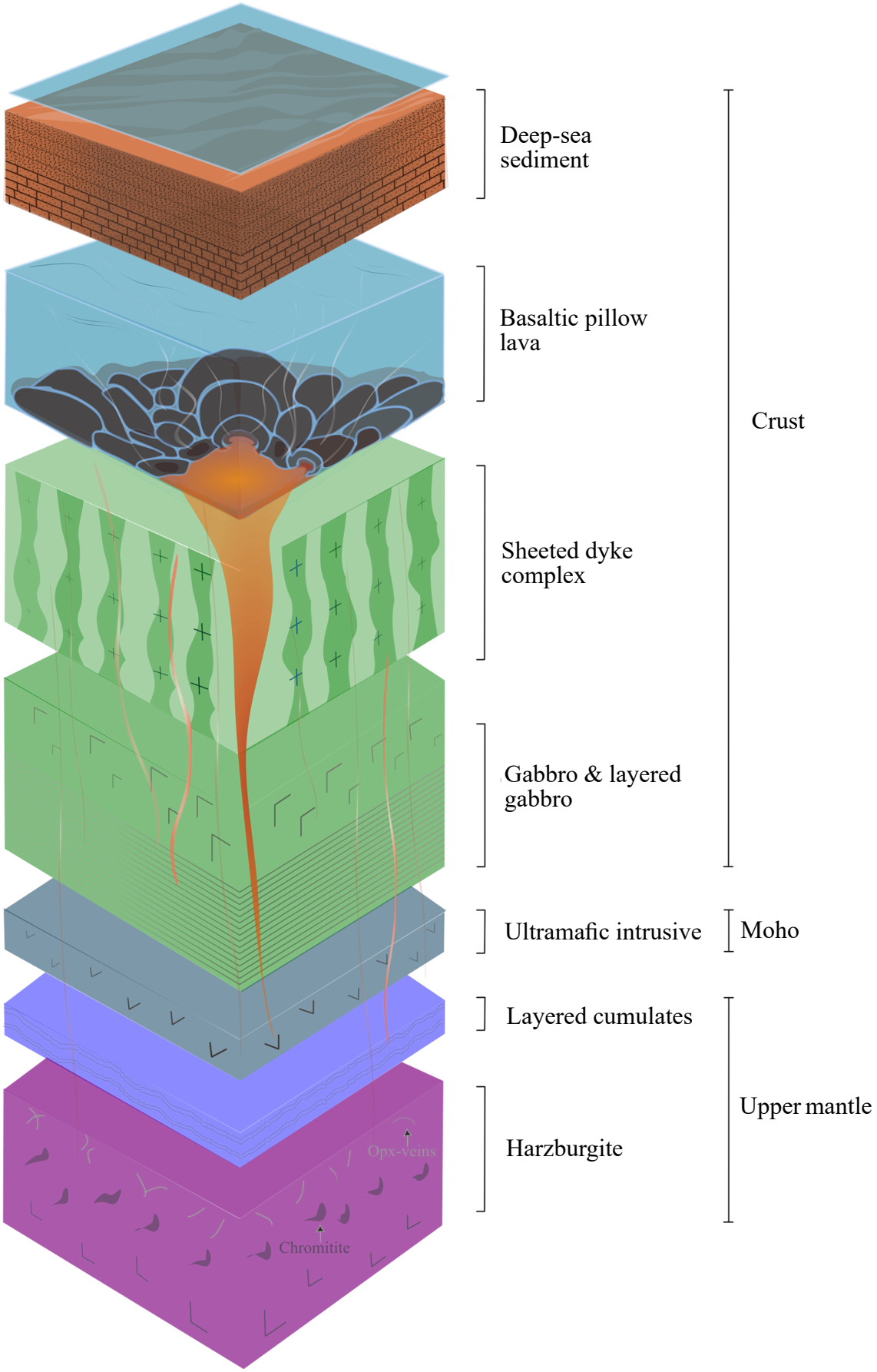

Fig. 7. A columnar section illustrating the upper mantle and crustal components of a generalized ophiolite complex.

DISCUSSION

The interaction between water and the eruption of hot magma (mostly mafic) on the seafloor creates a unique ellipsoid structure known as "Pillow Lava" (Buddington, 1926; Griffiths and Fink, 1992). Pillow lavas are typically formed at constructive plate boundaries of MORs; (De Boer et al., 1969). Their significance lies in being a crucial component of the upper section of the ophiolite sequence (Fig. 7), and they are genetically linked to the sheeted dyke found within the ophiolite (Dilek and Furnes, 2014). In the case of the pillow lavas found in the BRO, they are frequently intercalated with hyaloclastites, while the surrounding pelagic sediments primarily consist of chert and carbonates. Additionally, in the field, these pillow lavas are often intersected by parallel dykes of various compositions, including plagiogranite, gabbro, and diabase.

Both binary and ternary diagrams have been effectively utilized to better understand the source of the studied samples and their geotectonic settings. For instance, in the Th-Hf/3-Nb/16 and Th-Zr/117-Nb/16 ternary plots from Wood (1980), the mafic extrusive rocks fall within the enriched mid-ocean ridge basalt (EMORB) field. However, a notable trend shows a shift from the Hf and Zr-rich NMORB towards the Th and Nb-rich within plate alkaline (WPA) field (see Figs. 6A, B). Additionally, a significant correlation between Ti and V is observed in the diagram of Shervais (1982), indicating the presence of ocean floor basalt (OFB; Fig. 6C). The ternary diagram of La/10-Y/15-Nb/8 (Cabanis and Lecolle, 1989) demonstrates geochemical characteristics similar to NMORB, evolving through EMORB with increased levels of both La and Nb and ultimately progressing towards the Nb-rich alkali field (Fig. 6D). The Th_N vs. Nb_N diagram (Saccani et al., 2015) illustrates that the oceanic basalts shown in Fig. 6C, originate from depleted compositions, such as NMORB, to progressively more enriched compositions like EMORB and ocean island basalt (OIB) (OFB; Fig. 6E). This highlights the variation in sample source composition and their melting degree in the depleted mantle. These geochemical characteristics align with the Th/Yb vs. Nb/Yb diagram by Pearce (2008), illustrated in Fig. 6F. The REE patterns of the studied samples show significant variation in LREE, while the HREE patterns remain relatively flat. This variation in REE could indicate the degree of melting at different depths involving garnet-poor sources (Fig. 5A). In Fig. 5A, the samples exhibit varying patterns, transitioning from LREE-depleted NMORB-like to enriched OIB-like compositions. This variation may suggest a potential mixing process that contributes to the formation of EMORB. These characteristics are further supported by other trace element features, such as an enrichment of HFSE (Ta, Nb, Hf, and Ti), indicating the presence of relatively juvenile mantle sources (Fig. 5B). Taken together, the geochemical features of the studied basaltic samples from BRO indicate subduction-unrelated sources, which align with previous studies (Furnes and Safonova, 2019; Jian et al., 2010).

The complete section of the ophiolite mélange discovered over the past decades in the BZ of the CAOB, includes ultramafic and mafic rocks, sheeted dykes, pillow lavas, and deep marine sediments (Badarch et al., 2002; Buchan et al., 2001, 2002; Tomurtogoo, 1989, 2014). Since its discovery, numerous authors have interpreted the BRO as one of the largest suture zones or its oceanic crust in the CAOB. The age of formation of this oceanic lithosphere was long considered as Ediacaran (ca. 569 Ma; Kepezhinskas et al., 1991) until the first decade of the 21st century. However, in 2010, the late Neoproterozoic ages were determined using the U-Pb isotopic method on zircons obtained from the magmatic complexes of its ophiolite in the BZ (Jian et al., 2010). They found that the youngest age of the BRO is defined by the age of plagiogranite (ca. 636 Ma). This suggests that the ocean likely opened during the Neoproterozoic (ca. 636-665 Ma; Jian et al., 2010; Kovach et al., 2005). The ages of the studied mafic extrusive rocks from the BRO are currently unclear; however, they might be older than the plagiogranite, which is approximately 636 Ma (Jian et al., 2010). It is common for these basalts to be crosscut by parallel dykes in the field. Additionally, these mafic extrusive rocks could be either younger than or the same

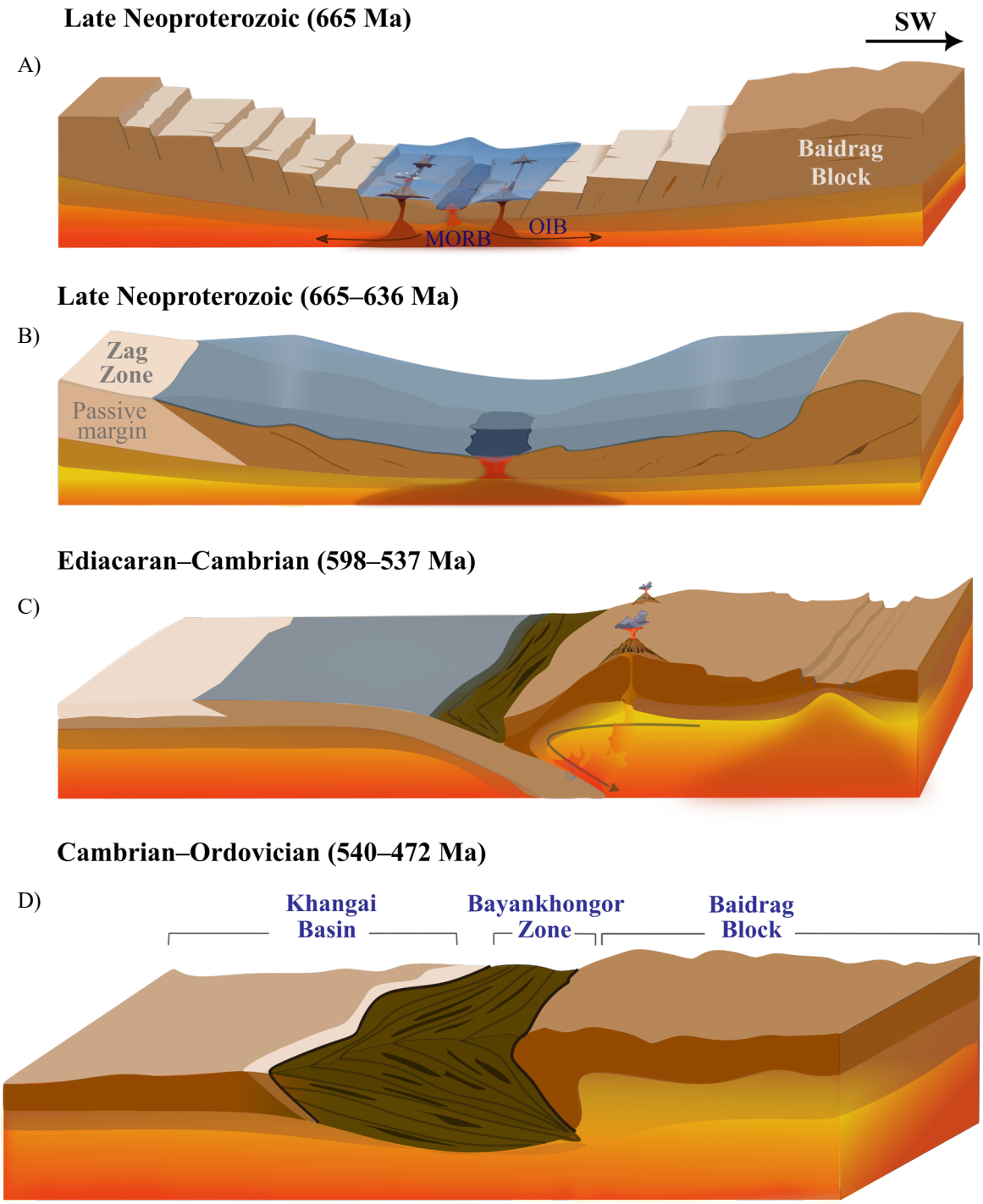

Fig. 8. The idealized tectonic models for the Bayankhongor region illustrate the formation of the Cryogenian oceanic crust and the Ediacaran supra-subduction, culminating in the final stage of accretionary orogeny and collision.

age as the mafic plutonic complexes, such as gabbro, which range from about 655 to 665 Ma (Jian et al., 2010; Kovach et al., 2005). Consequently, we propose an idealized tectonic models based on the pre-existing works and our new data (Fig. 8) that illustrate the formation of the Cryogenian oceanic crust (Figs. 8A, B) and Ediacaran-Cambrian supra-subduction (Fig. 8C), ultimately leading to the final stages of accretionary orogeny and early Cambrian-Ordovician amalgamation (Fig. 8D).

CONCLUSION

The studied 14 basaltic samples exhibit geochemically uniform characteristics, similar to those of basalts from the MORs. Therefore, we draw the following conclusions:

1) The studied samples primarily display

pillow-like structures in the field and are found in various forms, such as boudins in the serpentinite mélange, among other. Compositionally, the basaltic samples are categorized into two types: subalkaline and alkaline.

2) The samples display a range of LREE, with concentration varying from relatively depleted to similar to those found in NMORB to higher concentration characteristics of enriched EMORB and OIB. This variation in LREE indicates that the source of the basaltic rocks may have originated from both depleted and enriched mantle sources. The transition from NMORB to OIB demonstrates the extent of mixing between mantle domains, which contributes to the formation of EMORB.
3) Consequently, geochemical data indicate that the mafic extrusive rocks represent the upper part of a section of the BRO that were formed within a MOR setting, suggesting a subduction-unrelated source.
4) Although the subduction-unrelated tectonic model is often preferred for the BRO, the possibility of a back-arc setting cannot be entirely ruled out. A recent revised study for the Bayankhongor Zone indicates that an active margin existed in the northeastern part of the BB during the Ediacaran. Therefore, to gain a complete understanding of the BRO, further research is necessary.

ACKNOWLEDGMENT

The grant project of the Mongolian Academy of Sciences (MAS) (Project Number: C24/57), titled “Study of Pillow Lava from the Bayankhongor Zone” is led by Turbold Sukhbaatar. We would like to express our gratitude to locals Sukhbaatar Badamdorj and Naranbaatar Purevsuren for their assistance during our field expedition, especially in sampling within the Bayankhongor region. We sincerely appreciate MAS for supporting young researchers by providing scientists from its internal institutions, along with their students, the opportunity to participate in this annual grant project. We extend our thanks to Prof. Claire for her valuable corrections. We also acknowledge both reviewers, as their comments significantly enhanced the quality of our work. The English edits were carried out by a qualified native speaker, and we are grateful to Batkhishig for her meticulous editorial work.

Statement of Author Contribution and Conflicts of Interest

The authors firmly affirm that they possess no financial interests or personal relationships that could be perceived as influencing the integrity of the findings and conclusions presented in this paper.

Bayarmaa Batsukh contributed to Writing - Original Draft, Visualization, Investigation, Data Curation, Methodology. Turbold Sukhbaatar was responsible for project administration, funding acquisition, supervision, conceptualization, and writing of the manuscript. Gerel Ochir contributed to manuscript review and editing. Oyunbold Sukhbaatar and Odgerel Dashdorjgochoo participated in field investigations and data collection.

REFERENCE

Badarch, G., Cunningham, W.D., Windley, B.F. 2002. A new terrane subdivision for Mongolia: Implications for the Phanerozoic crustal growth of Central Asia. Journal of Asian Earth Science, vol. 21(1), p. 87-110. https://doi.org/10.1016/S1367-9120(02)00017-2

Boynton, W.V. 1984. Geochemistry of rare earth elements: Meteorite studies. In: Henderson, P. (Ed), Rare Earth Element Geochemistry, Elsevier, New York, vol. 63, p. 114. https://doi.org/10.1016/B978-0-444-42148-7.50008-3

Buchan, C., Cunningham, D., Windley, B.F., Tomurhuu, D. 2001. Stuctural and lithological characteristics of the Bayankhongor ophiolite zone, Central Mongolia. Journal of the Geological Society, vol. 158, p. 445-460. https://doi.org/10.1144/jgs.158.3.445

Buchan, C., Pfänder, J., Kröner, A., Brewer, T.S., Tomurtogoo, O., Tomurhuu, D., Cunningham, D., Windley, B.F. 2002. Timing of accretion and collisional deformation in the Central Asian Orogenic Belt: Implications of granite geochronology in the Bayankhongor

Ophiolite Zone. Chemical Geology, vol. 192(1-2), p. 23-45. https://doi.org/10.1016/S0009-2541(02)00138-9

Buddington, A.F.1926. Submarine Pillow Lavas of South-Eastern Alaska. The Journal of Geology, vol. 34(8) , p. 824-828. https://doi.org/10.1086/623369

Cabanis, B., Lecolle, M. 1989. The La/10-Y/15-Nb/8 diagram: A tool for distinguishing volcanic series and discovering crustal mixing and/or contamination: Comptes Rendus de l'Academie des Sciences, serie 2. Science de la Terre, vol. 309(20), p. 20. (in French)

De Boer, J., Schilling, J.G., Krause, D.C. 1969. Magnetic Polarity of Pillow Basalts from Reykjanes Ridge. Science, vol. 166(3908), p. 996-998. https://doi.org/10.1126/science.166.3908.996

Demoux, A., Kröner, A., Badarch, G., Jian, P., Tomurhuu, D., Wingate, M.T.D. 2009. Zircon Ages from the Baydrag Block and the Bayankhongor Ophiolite Zone: Time Constraints on Late Neoproterozoic to Cambrian Subduction- and Accretion-Related Magmatism in Central Mongolia. The Journal of Geology, vol. 117(4), p. 377-397. https://doi.org/10.1086/598947

Dilek, Y., Furnes, H. 2014. Ophiolites and Their Origins. Elements, vol. 10(2), p. 93-100. https://doi.org/10.2113/gselements.10.2.93

Furnes, H., Safonova, I. 2019. Ophiolites of the Central Asian Orogenic Belt: Geochemical and petrological characterization and tectonic settings. Geoscience Frontiers, vol. 10(4), p. 1255-1284. https://doi.org/10.1016/j.gsf.2018.12.007

Griffiths, R.W., Fink, J.H. 1992. The morphology of lava flows in planetary environments: predictions from analog experiments. Journal of Geophysical Research: Solid Earth, vol. 97(B13), p. 19739-19748. https://doi.org/10.1029/92jb01953

Janoušek, V., Farrow, C.M., Erban, V. 2006. Interpretation of whole-rock geochemical data in igneous geochemistry: introducing Geochemical Data Toolkit (GCDkit). Journal of Petrology, vol. 47(6), p. 1255-1259. https://doi.org/10.1093/petrology/egl013

Jahn, B.M., Capdevila, R., Liu, D., Vernon, A., Badarch, G. 2004. Sources of Phanerozoic granitoids in the transect Bayanhongor-Ulaan Baatar, Mongolia: geochemical and Nd isotopic evidence, and implications for Phanerozoic crustal growth. Journal of Asian Earth Sciences, vol. 23(5), p. 629-653. https://doi.org/10.1016/S1367-9120(03)00125-1

Jian, P., Kröner, A., Windley, B.F., Shi, Y., Zhang, F., Miao, L., Tomurhuu, D., Zhang, W., Liu, D. 2010. Zircon ages of the Bayankhongor ophiolite mélange and associated rocks: Time constraints on Neoproterozoic to Cambrian accretionary and collisional orogenesis in Central Mongolia. Precambrian Research, vol. 177(1-2), p. 162-180. https://doi.org/10.1016/j.precamres.2009.11.009

Jian, P., Kröner, A., Jahn, B.M., Windley, B.F., Shi, Y., Zhang, W., Zhang, F., Miao, L., Tomurhuu, D., Liu, D. 2014. Zircon dating of Neoproterozoic and Cambrian ophiolites in West Mongolia and implications for the timing of orogenic processes in the central part of the Central Asian Orogenic Belt. Earth-Science Reviews, vol. 133, p. 62-93. https://doi.org/10.1016/j.earscirev.2014.02.006

Kepezhinskas, P.K., Kepezhinskas, K.B., Pukhtel, I.S. 1991. Lower Paleozoic oceanic crust in Mongolian Caledonides: Sm-Nd isotope and trace element data. Geophysical Research Letters, vol. 18(7), p. 1301-1304. https://doi.org/10.1029/91GL01643

Kovach, V.P., Ping, J., Yarmolyuk, V.V., Kozakov, I.K., Liu, D., Terent'eva, L.B., Lebedev, V.I., Kovalenko, V.I. 2005. Magmatism and geodynamics of early stage of the Paleo-Asian Ocean formation: Geochronological and geochemical data on the ophiolites of the Bayan-Khongor zone. Doklady Akademii Nauk-Rossijskaya Akademiya Nauk, vol. 404, p. 229-234. (in Russian)

Parfenov, L.M., Berzin, N.A., Khanchuk, A.I., Badarch, G., Belichenko, V.G., Bulgatov, A.N., Dril, S.I., Kirillova, G.L., Kuzmin, M.I., Nokleberg, W., Prokopiev, A.V., Timofeev, V.F., Tomurtogoo, O., Yan, H. 2003. A model for the formation of orogenic belts of central and northeast Asia. Tikhookeanskaya geologiya, vol. 22, p. 7-41. (in Russian)

Pearce, J.A. 1996. A user's guide to basalt

discrimination diagrams. In: D.A. Wyman (Ed), Trace Element Geochemistry of Volcanic Rocks: Applications for Massive Sulphide Exploration. Geological Association of Canada, Short Course Notes, vol. 12, p. 79-113.

Pearce, J.A., Stern, R.J. 2006. Origin of back-arc basin magmas: Trace element and isotope perspectives. In: Christie, D.M., Fisher, C.R., Lee, S.-M., Givens, S. (Eds), Back-Arc Spreading Systems: Geological, biological, chemical, and physical interactions, vol. 166, p. 63-86. https://doi.org/10.1029/166GM06

Pearce, J.A. 2008. Geochemical fingerprinting of oceanic basalts with applications to ophiolite classification and the search for Archean oceanic crust. Lithos, vol. 100(1-4), p. 14-48. https://doi.org/10.1016/j.lithos.2007.06.016

Pearce, J.A. 2014. Immobile Element Fingerprinting of Ophiolites, Elements, vol. 10(2), p. 101-108. https://doi.org/10.2113/gselements.10.2.101

Ross, P.S., Bédard, J.H. 2009. Magmatic affinity of modern and ancient subalkaline volcanic rocks determined from trace-element discriminant diagrams. Canadian Journal of Earth Sciences, vol. 46(11), p. 823-839. https://doi.org/10.1139/E09-054

Saccani, E., Dilek, Y., Marroni, M., Pandolfi, L. 2015. Continental margin ophiolites of Neotethys: remnants of ancient ocean-continent transition zone (OCTZ) lithosphere and their geochemistry, mantle sources and melt evolution patterns. Episodes vol. 38(4), p. 230-249. https://doi.org/10.18814/epiiugs/2015/v38i4/82418

Şengör, A.M.C., Sunal, G., Natal'in, B.A., van der Voo, R. 2022. The Altaids: A review of twenty-five years of knowledge accumulation. Earth-Science Reviews, vol. 228, p. 104013. https://doi.org/10.1016/j.earscirev.2022.104013

Şengör, A.M.C., Natal'In, B.A., Burtman, V.S. 1993. Evolution of the Altaid tectonic collage and Palaeozoic crustal growth in Eurasia. Nature, vol. 364, p. 299-307. https://doi.org/10.1038/364299a0

Sukhbaatar, T., Schulmann, K., Janoušek, V., Soejono, I., Lexa, O., Míková, J., Hora, J.M., Song, D., Xiao, W., Poujol, M., Onongoo, T., Dashdorjgochoo, O., Zeng, H. 2024. Magmatic and sedimentological arguments for an Ediacaran active margin in the Bayankhongor Zone in western Mongolia, Central Asian Orogenic Belt. Gondwana Research, vol. 134, p. 385-409. https://doi.org/10.1016/j.gr.2024.07.017

Sun, S.S., McDonough, W.F. 1989. Chemical and isotopic systematics of oceanic basalts: Implications for mantle composition and processes. In: Saunders, A.D., Norry, M. (Eds), Magmatism in the Ocean Basins. Geological Society, London, Special Publications, vol. 42, p. 313-345. https://doi.org/10.1144/GSL.SP.1989.042.01.19

Shervais, J.W. 1982. Ti-V plots and the petrogenesis of modern and ophiolitic lavas. Earth and Planetary Science Letters, vol. 59(1), p. 101-118. https://doi.org/10.1016/0012-821X(82)90120-0

Terent'eva, L.B., Kovach, V.P., Yarmolyuk, V.V., Kovalenko, V.I., Kozlovsky, A.M. 2008. Composition, sources, and geodynamics of rock formation in the late riphean bayankhongor ophiolite zone: Characteristics of early stages in the evolution of the paleo-asian ocean. Doklady Earth Sciences, vol. 423, p. 1462-1466. https://doi.org/10.1134/S1028334X08090316

Terent'eva, L.B., Kozakov, I.K., Yarmolyuk, V.V., Anisimova, I.V., Kovach, V.P., Kozlovskii, A.M., Kudryashova, E.A., Sal'nikova, E.B., Yakovleva, S.Z., Fedoseenko, A.M., Plotkina, Y.V. 2010. Convergent processes in the evolution of the early caledonian Bayan-Khongor zone of Central Asia: Evidence from geological and geochronological investigations of the Khan-Ula gabbroid pluton. Doklady Earth Sciences, vol. 433, p. 937-943. https://doi.org/10.1134/S1028334X10070202

Tomurtogoo, O., 1989. Ophiolites and Formation of Folded Belts in Mongolia. Unpublished PhD Thesis. Russian Academy of Sciences, Moscow (in Russian)

Tomurtogoo, O., 2014. Tectonics of Mongolia. In: Petrov, O.V., Leonov, Yu.G., Tingdong, Li., Tomurtogoo, O. (Eds), Tectonics of northern, central, and eastern Asia: Explanatory note to the tectonic map of

northern central eastern Asia and adjacent areas at scale 1: 2500000. Saint Petersburg, Russia, p. 110-126.

Wakabayashi, J., Dilek, Y. 2003. What constitutes 'emplacement' of an ophiolite?: mechanisms and relationship to subduction initiation and formation of meta- morphic soles. In: Dilek, Y., Robinson, P.T. (Eds), Ophiolites in Earth History. Special Publications, Geological Society, London, vol. 218, p. 427-447. https://doi.org/10.1144/GSL.SP.2003.218.01.22

Whitney, D.L., Evans, B.W. 2010. Abbreviations for names of rock-forming minerals. American mineralogist, vol. 95(1), p. 185-187. https://doi.org/10.2138/am.2010.3371

Windley, B.F., Alexeiev, D., Xiao, W., Kröner, A., Badarch, G. 2007. Tectonic models for accretion of the Central Asian Orogenic Belt. Journal of the Geological Society, vol. 164, p. 31-47. https://doi.org/10.1144/0016-76492006-022

Winchester, J.A., Floyd, P.A. 1977. Geochemical discrimination of different magma series and their differentiation product using immobile elements. Chemical geology, vol. 20, p. 325-343. https://doi.org/10.1016/0009-2541(77)90057-2

Wood, D.A. 1980. The application of a Th–Hf–Ta diagram to problems of tectonomagmatic classification and to establishing the nature of crustal contamination of basaltic lavas of the British Tertiary volcanic province. Earth and planetary science letters, vol. 50(1), p. 11-30. https://doi.org/10.1016/0012-821X(80)90116-8

Xiao, W.J., Windley, B.F., Sun, S., Li, J., Huang, B., Han, C., Yuan, C., Sun, M., Chen, H. 2015. A tale of amalgamation of three Permo-Triassic collage systems in central Asia: Oroclines, sutures, and terminal accretion. Annual review of earth and planetary sciences, vol. 43, p. 477-507. https://doi.org/10.1146/annurev-earth-060614-105254

Xiao, W., Windley, B.F., Han, C., Liu, W., Wan, B., Zhang, J., Ao, S., Zhang, Z., Song, D. 2018. Late Paleozoic to early Triassic multiple roll-back and oroclinal bending of the Mongolia collage in Central Asia. Earth-Science Reviews, vol. 186, p. 94-128. https://doi.org/10.1016/j.earscirev.2017.09.020

Yarmolyuk, V.V., Kozlovsky, A.M., Travin, A.V., Kirnozova, T.I., Fugzan, M.M., Kozakov, I.K., Plotkina, Y.V., Eenjin, G., Oyunchimeg, T., Sviridova, O.E. 2019. Duration and Geodynamic Nature of Giant Central Asian Batholiths: geological and geochronological studies of the Khangai Batholith. Stratigraphy and Geological Correlation, vol. 27, p. 73-94. https://doi.org/10.1134/S0869593819010088

Zonenshain, L.P. 1973. The evolution of Central Asiatic geosynclines through sea-floor spreading. Tectonophysics, vol. 19(3), p. 213-232. https://doi.org/10.1016/0040-1951(73)90020-6

Zorin, Y.A. 1999. Geodynamics of the western part of the Mongolia-Okhotsk collisional belt, Trans-Baikal region (Russia) and Mongolia. Tectonophysics, vol. 306(1), p. 33-56. https://doi.org/10.1016/S0040-1951(99)00042-6